Progress In Electromagnetics Research M, Vol. 35, 113–120, 2014

Translational Motion Compensation Techniques in ISAR Imaging for Target with Micro-Motion Parts

Bin Yuan*, Shiyou Xu, and Zengping Chen

Abstract—In inverse synthetic aperture radar (ISAR) imaging, micro-motion structures on the target will induce additional time-varying frequency modulations to the radar echoes. Due to the disturbance of these mechanical vibration or rotation parts, it will be difficult to obtain a well-focused ISAR image of the target using conventional translational motion compensation methods. To solve this problem, two improved translational motion compensation techniques have been proposed in this paper. Firstly, the power transform is used in the range bin alignment processing to depress the disturbance of the micro-motion parts. Then, an improved autofocusing methods based on range bins selection is presented, which only uses the range bins of the radar returns from the main body scatterers for the phase adjustment. The imaging results from the measured data are given to verify the validity of the improved translational motion compensation techniques proposed in this paper.

1. INTRODUCTION

In conventional ISAR imaging, target is assumed to have rigid-body motion, and a well-focused ISAR image of the target is obtained via range-Doppler algorithm after removing the translational motion. In real-world situations, plentiful non-rigid-body targets are often present such as helicopters with rotating blades and airplanes with propellers or turbofans. Recent researches indicate that these mechanical vibration or rotation structures on the target will induce additional frequency modulations to the regular Doppler shift caused by the main body of the target in the radar returns, which is called "micro-Doppler (m-D) effect" [1].

On the one hand, the m-D phenomenon could be regarded as a unique signature of the target with micro-motions and provide additional information for target classification and recognition [2–4]. On the other hand, the m-D may contaminate the ISAR image of the main body of the target. In order to gain a more focused image of the target, the separation of m-D is required. According to literatures published, several available m-D extraction and ISAR imaging techniques have been proposed [5–8]. But, unfortunately all these m-D extraction and ISAR imaging researches worked with the assumption that the target is rigid, and ignore the disturbance for the translational motion compensation in the ISAR imaging induced by the micro-motion parts of the target.

As a matter of fact, the conventional translational motion compensation methods may incompetent at the autofocusing in the ISAR imaging for targets with micro-motion structures. To solve this problem, two techniques as modified approaches of the conventional translational motion compensation are proposed. Firstly, in range bin alignment step, a power transform is used to reduce the variational scope of the amplitude of the micro-motion parts echoes in the range profiles, and to improve the similarity of the range profiles. Secondly, a phase adjustment method based on adaptive selection of range bins is presented. By range bins selection, we only utilize the returns of the main body to

Received 15 January 2014, Accepted 16 March 2014, Scheduled 19 March 2014

* Corresponding author: Bin Yuan (yuanbin_163@163.com).

The authors are with the ATR National Defense Science and Technology Key Laboratory, National University of Defense Technology, Changsha 410073, China.

estimate the phase error, which may avoid the disturbance from the rotating parts and improve the phase adjustment accuracy in ISAR imaging.

The remainder of this paper is organized as follows. The radar echoes of the target with micro-motion parts are modeled in Section 2. In Section 3, two techniques as an improved approaches of the conventional translational motion compensation for targets with micro-motion parts is given. The results from the measured data are given in Section 4, and the final part is the conclusions.

2. SIGNAL MODEL OF TARGETS WITH MICRO-MOTION PARTS

Without loss of generality, this paper considers the imaging model of the target with micro-motion parts on a 2-D imaging plane. Taking the target with rotating parts, for example, the geometry of the target is shown in Fig. 1. In this figure, the imaging plane of target is denoted as XOY, the local coordinate for the rotating parts denoted as xoy, and p and q denote the scatterer from the main body and the rotating parts of target, respectively. The main body scatterer p rotates around the imaging center O with angular velocity ω_p. The rotating radius is r_p, and the initial angle is θ_p. The rotating parts scatterer q rotates around the local coordinate center o with angular velocity ω_q. The rotating radius is r_q, and the initial angle is θ_q. The distance between the imaging center O and the local coordinate center o is r_o, and the initial angle of local coordinate center o in the coordinate XOY is θ_o. In addition, the distance from the radar to the imaging center is R_O.

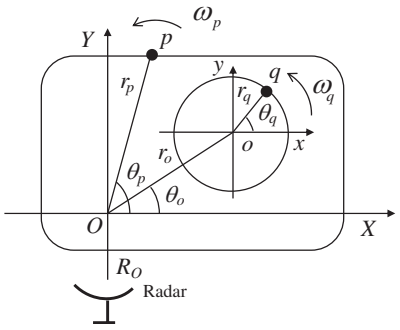

Figure 1. Geometry for micro-motion targets with rotating parts.

In practice, in order to increase the radar transmit power and decrease the receiver bandwidth, the radar usually transmits a linear frequency modulation (LFM) signal and then dechirps the received signal. The expression of the transmitted chirp signal is

$$s\left(\hat{t}, t_m\right) = rect\left(\frac{\hat{t}}{T_{pul}}\right) \exp\left\{j2\pi\left[f_c t + \frac{1}{2}\gamma\hat{t}^2\right]\right\} \tag{1}$$

where

$$rect\left(\frac{\hat{t}}{T_{pul}}\right) = \begin{cases} 1, & \left|\hat{t}\right| \le T_{pul}/2 \\ 0, & \left|\hat{t}\right| > T_{pul}/2 \end{cases} \tag{2}$$

denotes the window function, f_c the carrier frequency, T_{pul} the chirp pulse duration, and γ the chirp rate.

The echoes of the target can be expressed as

$$\begin{aligned} S_r\left(\hat{t}, t_m\right) &= S_p\left(\hat{t}, t_m\right) + S_q\left(\hat{t}, t_m\right) \\ &= \sum_{p=1}^{P} \sigma_p rect\left(\frac{\hat{t} - 2R_p(t_m)/c}{T_{pul}}\right) \exp\left\{j2\pi\left[f_c(\hat{t} - \frac{2R_p(t_m)}{c}) + \frac{1}{2}\gamma(\hat{t} - \frac{2R_p(t_m)}{c})^2\right]\right\} \\ &\quad + \sum_{q=1}^{Q} \sigma_q rect\left(\frac{\hat{t} - 2R_q(t_m)/c}{T_{pul}}\right) \exp\left\{j2\pi\left[f_c(\hat{t} - \frac{2R_q(t_m)}{c}) + \frac{1}{2}\gamma(\hat{t} - \frac{2R_q(t_m)}{c})^2\right]\right\} \end{aligned} \tag{3}$$

where $R_p(t_m)$ and $R_q(t_m)$ are the distance from the radar to the main body scatterer and the rotating parts scatterer, respectively; σ_p and σ_q are scattering coefficients of the main body scatterer and the rotating parts scatterer, respectively.

After the process of dechirping, the compressed signal can be written as

$$\begin{aligned} S_v\left(\hat{t}, t_m\right) &= \sum_{m=1}^{M} \sigma_m \exp\left\{-j\frac{4\pi\gamma}{c}\hat{t}\Delta R_p(t_m)\right\} \exp\left\{-j\frac{4\pi f_c}{c}\Delta R_p(t_m)\right\} \\ &\quad + \sum_{n=1}^{N} \sigma_n \exp\left\{-j\frac{4\pi\gamma}{c}\hat{t}\Delta R_q(t_m)\right\} \exp\left\{-j\frac{4\pi f_c}{c}\Delta R_q(t_m)\right\} \end{aligned} \tag{4}$$

where $\Delta R_p(t_m) = R_p(t_m) - R_{ref}(t_m)$ and $\Delta R_q(t_m) = R_q(t_m) - R_{ref}(t_m)$ are the instantaneous ranges from the reference point to p and q, respectively, and $R_{ref}(t_m)$ is the range of the reference point used in the dechirping signal.

The instantaneous distance between the main body scatterer and the reference point satisfies

$$\Delta R_p(t_m) = r_p \sin(\omega_p t_m + \theta_p) + r_e(t_m) \tag{5}$$

where $r_e(t_m)$ is the range error from imaging center to reference point in the dechirping signal.

Whereas, for the rotating structure, the distance between the rotating parts scatterer and the reference point can be expressed as

$$\Delta R_q(t_m) = r_o \sin(\omega_o t_m + \theta_o) + r_q \sin(\omega_q t_m + \theta_q) + r_e(t_m) \tag{6}$$

By taking Fast Fourier transform (FFT) of $S_v\left(\hat{t}, t_m\right)$ along the fast time, it is easy to get the range information of the target, and thus different range cells can be distinguished separately. Therefore, after range compression in the fast-time domain, the radar signal through a fixed range cell r is given by

$$\begin{aligned} S(r, t_m) &= \sum_{p=1}^{P} \sigma_p T_{pul} \mathrm{sinc}\left\{T_{pul}\left[r - \frac{2\gamma}{c}\Delta R_p(t_m)\right]\right\} \exp\left\{-j\frac{4\pi f_c}{c}\Delta R_p(t_m)\right\} \\ &\quad + \sum_{q=1}^{Q} \sigma_q T_{pul} \mathrm{sinc}\left\{T_{pul}\left[r - \frac{2\gamma}{c}\Delta R_q(t_m)\right]\right\} \exp\left\{-j\frac{4\pi f_c}{c}\Delta R_q(t_m)\right\} \end{aligned} \tag{7}$$

Because the range error exists in the process of dechirping and because the phase error in the transmit is random in nature, the received signal is not coherent. Following the range compression, translational motion compensation should be done to achieve good performance of ISAR imaging.

3. TRANSLATIONAL MOTION COMPENSATION TECHNIQUES FOR TARGETS WITH MICRO-MOTION PARTS

The translational motion compensation in ISAR imaging is generally divided into two steps: the range bin alignment and the phase adjustment. The range alignment is performed to align the high resolution range profiles in the range direction, so that the returns of different pulses from the same scatterer lie in the same range cell. The phase adjustment removes the residual phase error by multiplying range aligned signals with the conjugate phase of a selected reference point.

However, these conventional translational motion compensation methods assume that the target is rigid, and whose scatterers' positions are almost fixed in the imaging interval. But, in real-world situations, non-rigid-bodies are often present such as rotating blades in helicopters, and propellers or turbofans in airplanes. Then, to obtain a well-focused ISAR image of the target, some modified translational motion compensation approaches should be researched.

3.1. Improved Range Bin Alignment Method Based on Power Transform

In the range alignment, signals from the same scatterer are aligned in the same range bin by shifting the echoes. If no prior knowledge is available about the translational motion of the target, typical methods

include the dominant scatter method [9], the maximum correlation method [9], the minimum entropy method [10], etc.

The dominant scatter method tracks a prominent scatter to estimates the range shift and is sensitive to target scintillation. If there is no prominent scatter on the target, the dominant scatter method cannot be carried out into execution. The minimum entropy method is robust to reflectivity scintillation. But, it has computational complexity. Maximum correlation method is a classic method, which aligns high-resolution range profiles by using the principle that the envelope correlation of two adjacent profiles reaches a maximum when they are aligned.

The maximum correlation method is achieved using the similarity of the envelopes of the echoes. Then, the traditional maximum correlation method is likely to fail when micro-motion structures are present on the target, as the similarity of the adjacent profiles is contaminated seriously. To depress the disturbance of the micro-motion structures and improve the similarity of the range profiles, a power transform is used to reduce the variational scope of the amplitude of the micro-motion parts echoes in the range profiles.

For two adjacent envelopes $S(r, t_m)$ and $S(r, t_{m+1})$, the range shift can be gained by

$$\tau = \arg\max S(r, t_m)^v S(r - \tau, t_{m+1})^v \tag{8}$$

where τ is the range shift, v the power transform coefficient, and $0 < v < 1$. If the average range profile is used, we get the range shift

$$\begin{cases} \tau = \arg\max S^*(r, t_m)^v S^*(r - \tau, t_{m+1})^v \\ S^*(r, t_{m+1}) = \eta S(r, t_m) + S(r, t_{m+1}) \end{cases} \tag{9}$$

where η is the weighted factor.

3.2. Improved Phase Error Correction Based on Range Bin Selection

If range alignment is done well, the phase adjustment is carried out to remove the phase error. According to published literatures, in phase adjustment step, there are various approaches such as the single dominant scatters algorithm [9], multiple dominant scatters algorithm [11], Doppler centroid tracking method [12], phase gradient method [13], minimum entropy method [14], and maximum contrast method [15]. The dominant scatters algorithm can be only implemented effectively when dominant scattering centers can be extracted from high-resolution range profiles. The minimum entropy method and maximum contrast method have high computation burden.

The conventional Doppler centroid tracking method and phase gradient method will perform well when the target is rigid. However, the presence of micro-motion structures brings inherent difficulty to track and compensate the phase error. It will degrade the accuracy of phase error estimation when traditional Doppler centroid tracking algorithm performs on each range bin in the profiles. Therefore, to choose some range bins which have the target's main body scatterers and to give up range bins which contain the target's micro-motion structures scatterers will improve the focus performance and accelerate the calculation speed.

During the imaging interval, small angle approximation can be assumed for the main body, which results in $\cos(\omega_p t_m) \approx 1$ and $\sin(\omega_p t_m) \approx \omega_p t_m$. The phase of the radar echoes from the main body scatterer can be written as

$$\Phi_p = \frac{4\pi f_c}{c} \Delta R_p(t_m) = \underbrace{\frac{4\pi}{\lambda}[x_p + y_p \omega_0 t_m]}_{\phi_p(t_m)} + \underbrace{\frac{4\pi}{\lambda}[r_e(t_m)]}_{\phi_c(t_m)} \tag{10}$$

where λ denotes the wave length, $\phi_p(t_m)$ the phase induced by main body scatterers, and $\phi_c(t_m)$ the phase error. Equation (10) shows that the phase variety of scatterers from the main body possess constant variety in each two adjacent echoes. Therefore, the phase error can be estimated with conventional Doppler centroid tracking method or phase gradient method.

However, small angle approximation does not hold for the rotating parts, since its rotation rate is usually much larger than that of the main body. The phase of the radar echoes from the rotating

structure scatterer of the target can be written as

$$\Phi_q(t_m) = \frac{4\pi f_c}{c}\Delta R_q(t_m) = \underbrace{\frac{4\pi}{\lambda}[x_o + y_o\omega_o t_m] + \frac{4\pi}{\lambda}[r_q\cos(\omega_q t_m + \theta_q)]}_{\phi_q(t_m)} + \underbrace{\frac{4\pi}{\lambda}[r_c(t_m)]}_{\phi_c(t_m)} \tag{11}$$

where $\phi_q(t_m)$ is the phase induced by micro-motion scatterers. In Equation (11), the first term of $\phi_q(t_m)$ is the phase caused by the rotation motion of the target which is constant during the imaging interval, and the second term of $\phi_q(t_m)$ represents the phase component induced by the quick rotation motion of the rotating part in addition to the target's bulk movement which is a sinusoidal frequency modulation (FM) signal. Then, it is difficult to estimate the phase error with conventional phase adjustment algorithms.

A feasible approach is only utilizing the radar returns of the main body to estimate the phase error, which may avoid the disturbance from the rotating parts and availably improve the phase adjustment accuracy in the ISAR imaging. It is well known that entropy function can be utilized to describe the involved information quantities of stochastics signal, and here, the entropy function is used to measure the variety degree of each range bin.

$$E(l) = -\sum_{k=1}^{K}\frac{|g(k,l)|^2}{S}\ln\left[\frac{|g(k,l)|^2}{S}\right] \tag{12}$$

$$S = \sum_{k=1}^{K}\sum_{l=1}^{L}|g(k,l)|^2 \tag{13}$$

where k means the k-th echo after motion compensation and l the l-th range bin.

The Doppler frequency induced by the main body can be written as

$$f_p = \frac{1}{2\pi}\frac{d(\phi_p(t_m))}{dt_m} = \frac{2}{\lambda}\frac{d(x_p + y_p\omega_0 t_m)}{dt_m} = \frac{2}{\lambda}\omega_p y_p \tag{14}$$

The Doppler frequency induced by the rotating structure of the target can be written as

$$f_q = \frac{1}{2\pi}\frac{d(\phi_q(t_m))}{dt_m} = \frac{2}{\lambda}\frac{d(r_q\cos(\omega_q t_m + \theta_q) + x_o + y_o\omega_o t_m)}{dt_m} = \frac{2}{\lambda}y_o\omega_o + \frac{2}{\lambda}r_q\omega_q\sin(\theta_q + \omega_q t_m) \tag{15}$$

The rotating parts may undergo many cycles while the main body rotates only a few degrees during the imaging interval. It is obvious that $\omega_p \ll \omega_q$, then, we can obtain the conclusion that if there are micro-motion structures scatterers in a range bin, the value of entropy will be greater; otherwise, the value will be less when only main body scatterers are in the range bins.

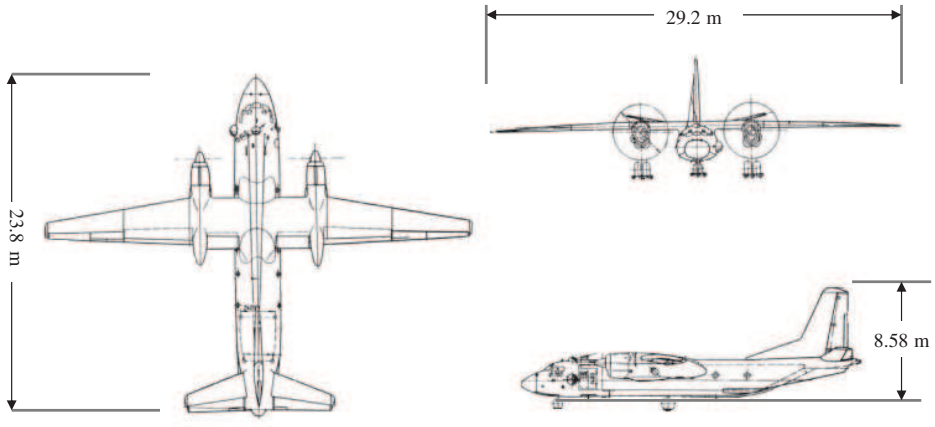

Figure 2. Framework for AN-26 plane.

4. EXPERIMENT AND PERFORMANCE ANALYSIS

The improved algorithm is applied to two sets of measured data. The first set is the measured data collected from an AN-26 aircraft. The second is the measured data collected from a Boeing-737 aircraft.

The AN-26 plane is a turboprop applied to short-range transportation with two turbos on each side of the airframe. The aircraft propellers are often visible to the radar and will provide a chopped reflection of the transmitting signal. The framework of the plane is shown in Fig. 2. The radar bandwidth is 400 MHz, and the pulse PRF is 400 Hz.

The Boeing-737 featured turbofan engines which place ahead of the wings, and by moving engine accessories to the sides of the engine pod which gives the plane a distinctive non-circular air intake. The fan blades of the engines are often partially or wholly hidden by the ducts, but in some cases the blades are visible to the radar. The framework of the plane is shown in Fig. 3. The radar bandwidth is 1 GHz, and the PRF is 1000 Hz.

Figures 4(a) and 4(b) show the ISAR image of AN-26 and Boeing 737 with range-Doppler algorithm after conventional translational motion compensation, respectively. The ISAR images with range-Doppler algorithm using the improved translational motion compensation techniques proposed in this paper are shown in Fig. 4(c) and Fig. 4(d). The results show that the improved translational motion compensation techniques can gain a more focused image of the target with micro-motion structures.

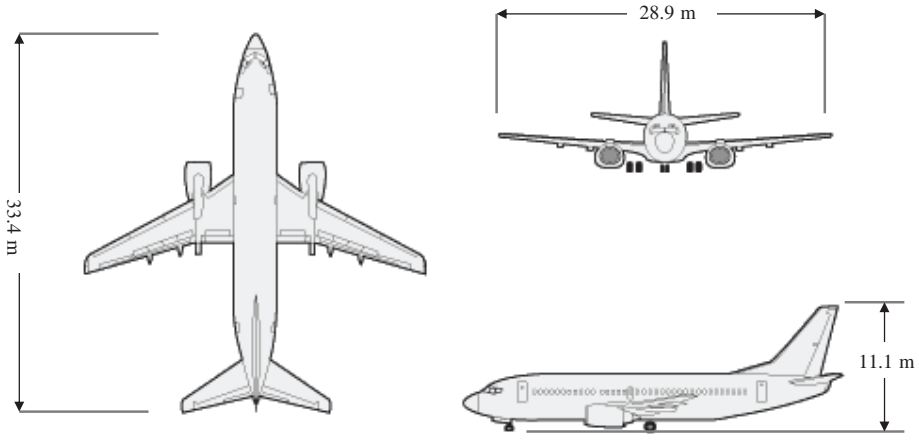

Figure 3. Framework for Boeing 737 plane.

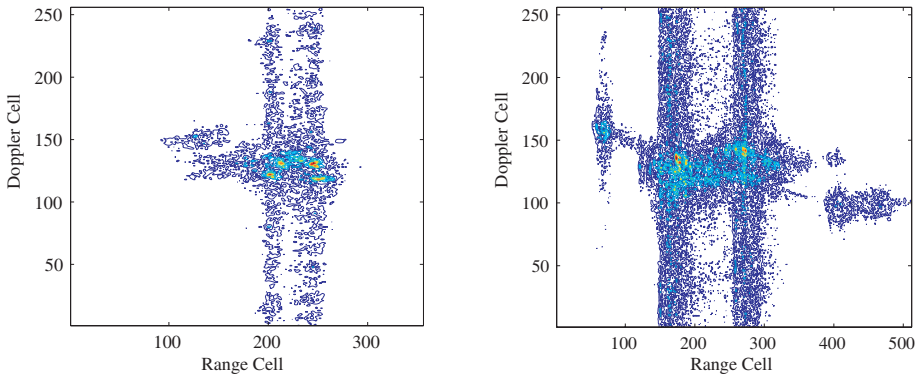

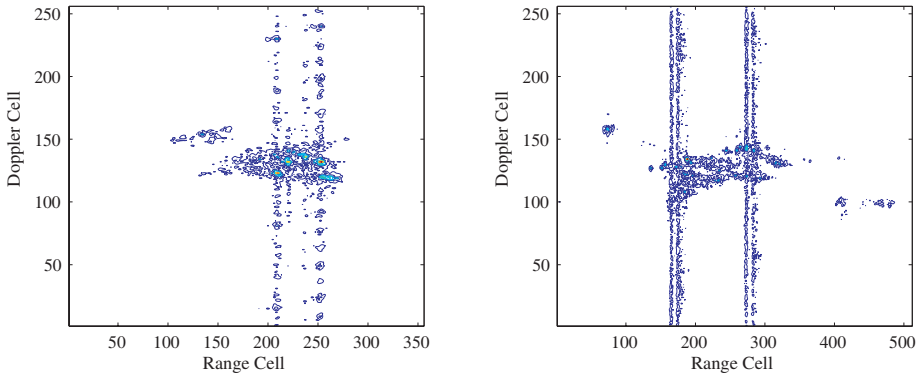

Figure 4. ISAR image of AN-26 and Boeing 737. (a) AN-26 ISAR image with the range-Doppler algorithm after conventional translational motion compensation. (b) Boeing 737 ISAR image with the range-Doppler algorithm after conventional translational motion compensation. (c) AN-26 ISAR image with range-Doppler algorithm using the improved translational motion compensation techniques. (d) Boeing 737 ISAR image with range-Doppler algorithm using the improved translational motion compensation techniques.

5. CONCLUSION

We present a novel improvement for ISAR autofocus of targets with micro-motion parts. In our improved algorithm, a power transform is used to reduce the variational scope of the amplitude of the micro-motion parts echoes in the range profiles, and to improve the similarity of the range profiles. Then, a adaptively evaluating and selecting range bins will avoid the influence of micro-motion scatterers, which cannot be well avoided using usual phase adjustment methods. Experiments on real data show the effectiveness and advantage of our improved translational motion compensation algorithm.

REFERENCES

1. Chen V. C., F. Y. Li, S. S. Ho, et al., "Micro-Doppler effect in radar: Phenomenon, model, and simulation study," *IEEE Trans. Aerosp. Electron. Syst.*, Vol. 42, No. 1, 2–21, 2006.
2. Chen, V. C., F. Y. Li, S. S. Ho, et al., "Analysis of micro-Doppler signatures," *Proc. Inst. Elect. Eng. — Radar Sonar Navig.*, Vol. 150, No. 4, 271–276, 2003.
3. Setlur, P., M. Amin, and T. Thayaparan, "Micro-Doppler signal estimation for vibrating and rotating targets," *Proc. 8th Int. Symp. Signal Process*, 639–642, Aug. 2005.
4. Thayaparan, T., E. Abrol, E. Riseborough, et al., "Analysis of radar micro-Doppler signatures from experimental helicopter and human data," *IET Radar Sonar Navig.*, Vol. 1, No. 4, 289–299, 2007.
5. Li, J. and H. Ling, "Application of adaptive chirplet representation for ISAR feature extraction from targets with rotating parts," *Proc. Inst. Elect. Eng. — Radar Sonar Navig.*, Vol. 150, No. 4, 284–291, 2003.
6. Stankovic, L., I. Djurovic, and T. Thayaparan, "Separation of target rigid body and micro-Doppler effects in ISAR imaging," *IEEE Trans. Aerosp. Electron. Syst.*, Vol. 42, No. 4, 1496–1506, 2006.
7. Bai, X., M. Xing, F. Zhou, et al., "Imaging of micromotion targets with rotating parts based on empirical-mode decomposition," *IEEE Trans. Geosci. Remote Sens.*, Vol. 46, No. 11, 3514–3523, 2008.
8. Yuan, B. and Z. Chen, "Micro-Doppler analysis and separation based on complex local mean decomposition for aircraft with fast rotating parts in ISAR imaging," *IEEE Trans. Geosci. Remote Sens.*, Vol. 52, No. 2, 1285–1298, 2014.
9. Chen, C. C., H. C. Andrews, and S. Xu, "Target motion induced radar imaging," *IEEE Trans. Aerospace Electron. Syst.*, Vol. 16, No. 1, 2–14, 1980.

10. Wang, J. and D. Kasilingam, "Global range alignment for ISAR," *IEEE Trans. Aerospace Electron. Syst.*, Vol. 39, No. 1, 351–357, 2003.
11. Wei, Y., T. S. Yeo, and B. Zheng, "Weighted least-squares estimation of phase error for SAR/ISAR autofocus," *IEEE Trans. Geosci. Remote Sens.*, Vol. 37, No. 5, 2487–2494, 1999.
12. Itoh, T. M. and G. W. Donohoe, "Motion compensation for ISAR via centroid tracking," *IEEE Trans. Aerospace Electron. Syst.*, Vol. 32, No. 7, 1191–1197, 1996.
13. Wahl, D. E., P. H. Eichel, D. C. Ghiglia, et al., "Phase gradient autofocus — A robust tool for high resolution SAR phase correction," *IEEE Trans. Aerospace Electron. Syst.*, Vol. 30, No. 3, 827–835, 1994.
14. Xi, L., L. Guosui, and J. Ni, "Autofocusing of ISAR images based on entropy minimization," *IEEE Trans. Aerospace Electron. Syst.*, Vol. 35, No. 4, 1240–1252, 1999.
15. Martorella, M., F. Berizzi, and B. Haywood, "Contrast maximization based technique for 2-D ISAR autofocusing," *IEE Proc., Radar Sonar Navig*, Vol. 152, No. 4, 253–262, 2005.